

## RECONSTRUCTING THE COSMIC EVOLUTION OF QUASARS FROM THE AGE DISTRIBUTION OF LOCAL EARLY-TYPE GALAXIES

ZOLTÁN HAIMAN

Department of Astronomy, Columbia University, 550 West 120th Street, New York, NY 10027, USA;  
zoltan@astro.columbia.edu

RAUL JIMENEZ & MARIANGELA BERNARDI

Department of Physics and Astronomy, University of Pennsylvania, 209 South 33rd Street, Philadelphia, PA 19104, USA;  
(raulj.bernardm)@physics.upenn.edu  
Draft version September 11, 2018

### ABSTRACT

We use the spectra of  $\approx 22,000$  nearby early-type galaxies from the Sloan Digital Sky Survey (SDSS) to determine the age distribution of these galaxies as a function of their velocity dispersion  $\sigma_v$  in the range  $100 \text{ km s}^{-1} \lesssim \sigma_v \lesssim 280 \text{ km s}^{-1}$ . We then combine the inferred age-distributions with the local abundance of spheroids, including early-type galaxies and late-type bulges, to predict the evolution of the quasar luminosity function (LF) in the redshift range  $0 < z \lesssim 6$ . We make the following simple assumptions: (i) the formation of stars in each galaxy, at the epoch identified with the mean mass-weighted stellar age, is accompanied by the prompt assembly of the nuclear supermassive black hole (SMBH); (ii) the mass of the SMBH obeys the  $M_{\text{bh}} - \sigma_v$  correlation observed in nearby galaxies; (iii) the SMBH radiates at a fraction  $f_{\text{Edd}}$  of the Eddington limit for a fixed duration  $t_Q$ , and is identified as a luminous quasar during this epoch, (iv) the intrinsic dispersions in the Eddington ratio and the  $M_{\text{bh}} - \sigma_v$  relation produce a combined scatter of  $\Delta \log L_Q$  around the mean logarithmic quasar luminosity  $\langle \log L_Q \rangle$  at fixed  $\sigma_v$ . These assumptions require that the SMBH remnants of quasars with  $L_{\text{bol}} \lesssim 10^{12.5} f_{\text{Edd}} L_{\odot}$  reside predominantly in bulges of late type galaxies. We find that evolution of the observed quasar LF can be fit over the entire redshift range in this simple model,  $0 < z \lesssim 6$  with the choices of  $0.6 \lesssim \Delta \log L_Q \lesssim 0.9$ ,  $6 \times 10^7 \text{ yr} \lesssim t_Q \lesssim 8 \times 10^7 \text{ yr}$ , and  $0.3 \lesssim \langle f_{\text{Edd}} \rangle \lesssim 0.5$ . We find no evidence that any of the model parameters evolves with redshift, supporting the strong connection between the formation of stars and nuclear SMBHs in spheroids.

*Subject headings:* quasars: general – galaxies: nuclei – galaxies: active – black hole physics – accretion

### 1. INTRODUCTION

The discovery of tight correlations between the masses of supermassive black holes (SMBHs) at the centers of galaxies and the global properties of the spheroid component of the galaxies themselves (see, e.g., Magorrian et al. 1998; Ferrarese & Merritt 2000; Gebhardt et al. 2000; Graham et al. 2001) have suggested a strong link between the formation of SMBHs and their host spheroids. Several groups have noted that galaxy formation and SMBH growth should be linked, and many modeled the joint cosmological evolution of quasars and galaxies (see, e.g., Monaco et al. 2000; Kauffmann & Haehnelt 2001; Haiman & Menou 2001; Granato et al. 2001; Ciotti & van Albada 2001, Cavaliere & Vittorini 2002; Lapi et al. 2006, and references therein).

A particularly revealing characteristic of this cosmic evolution is the so-called “downsizing”. Observations have long suggested an inverse correlation between the ages of elliptical galaxies and their size, with more massive ellipticals forming at earlier epochs (e.g., Heavens et al. 2004 and references therein). Interestingly, the characteristic quasar luminosity similarly declines over time from  $z \approx 2$  to  $z = 0$  (Boyle et al. 2000). At first sight, the decline of both the characteristic galaxy velocity dispersion, and of quasar luminosity, is surprising in “bottom-up” hierarchical structure formation models. This anti-hierarchical behavior, can nevertheless be naturally accommodated in these structure formation models, invoking the energy feedback from the AGN on the host galaxy (e.g. Granato et al. 2004) and large-scale environmental effects (e.g. Blanton et al. 1999). The similarity between the “downsizing” observed for elliptical galaxies and for quasars has been noted in previous work (e.g. Franceschini et al. 1999; Haiman, Ciotti & Ostriker 2004), and, as these works pointed out, it suggests that the formation of

SMBHs and spheroids was linked by the same physical mechanism at all cosmic epochs.

The simplest hypothesis to interpret the above trends is that star formation in spheroids and BH fueling are proportional to one another at all times (Haiman, Ciotti & Ostriker 2004). With the additional assumptions that BH accretion luminosity stays at some fraction of the Eddington limit during luminous quasar phases, and that these phases have a characteristic duty cycle, one can predict the evolution of quasars from the evolution of early-type galaxies (and vice versa). Unfortunately, a direct observational test of the above hypotheses is not possible, as the cosmic evolution of the population of early-type galaxies has not been determined from observations out to high  $z$ .

Here we follow an alternative “archaeological” approach, and we use age-distributions we infer for nearby early-type galaxies, as a function of their velocity dispersion, to reconstruct in detail the evolution of quasars, as a function of their luminosity. This approach has been attempted previously by Cattaneo & Bernardi (2003), who have used the mean age of early-type galaxies vs their velocity dispersion, together with assumptions about the geometry of obscuring tori, to infer the evolution of their abundance, and to predict the evolution of the quasar LF (see also Granato et al. 2001 for the inverse approach). In this paper, we improve on these previous studies in several ways: (i) we infer the age distribution, rather than only the mean age, as a function of  $\sigma_v$ , for early type galaxies, (ii) we include the population of late-type bulges in our analysis, which indeed dominate the spheroid population at low velocity dispersion, (iii) we perform a quantitative statistical comparison between the predicted and observed quasar LFs, and (iii) the quasar lifetime, the mean Eddington ratio of SMBHs, and its scatter, are taken as three fitting parameters that are fit simultaneously. We find that the shape of the quasar LF we predict is in

rough agreement with observations, without introducing either a luminosity-dependent obscuration or a redshift-evolution of either of the three model parameters. Our results require that the quasar luminosity  $L_Q$  has a non-negligible scatter (of  $\gtrsim 0.5$  dex) at a fixed value  $\sigma_v$  of the host galaxy.

The rest of this paper is organized as follows. In § 2, we discuss the sample of early type galaxies we used in our analysis, and infer the age distribution of these galaxies. In § 3, we discuss our modeling that converts the inferred age-distributions to the evolution of the quasar luminosity function (LF). In § 4, we discuss our method of statistically comparing the predicted and observed quasar LFs. In § 5, we present and discuss our main results, and in § 6, we briefly summarize our conclusions. Throughout this paper, we adopt the background cosmological parameters  $\Omega_m = 0.3$ ,  $\Omega_\Lambda = 0.7$ , and  $H_0 = 70 \text{ km s}^{-1} \text{ Mpc}^{-1}$ , consistent with the values measured recently by the *WMAP* experiment (Spergel et al. 2006).

## 2. THE AGE DISTRIBUTION OF EARLY-TYPE GALAXIES

We have used the sample of early-type galaxies obtained by Bernardi et al. (2006a). The sample, extracted from the Sloan Digital Sky Survey (York et al. 2000), contains over 40,000 early-type galaxies selected for having apparent magnitude  $14.5 \leq g \leq 17.75$  with spectroscopic parameter  $e_{class} < 0$ , which gives a PCA component corresponding to no emission lines, and  $fracDev_r > 0.8$ , which is a seeing-corrected indicator of morphology. Only those objects were included that have measured velocity dispersions, which translates in the spectra having  $S/N > 10$  in the region  $4200 - 5800 \text{ \AA}$ . The sample extends over a redshift range  $0.013 < z < 0.25$ , which corresponds to a maximum look-back time of 3 Gyr.

We computed the ages of the galaxies in three different ways. First, for each individual galaxy, we fitted a single stellar population model to the whole observed spectrum (continuum+lines) with two parameters: age and metallicity. Second, we used the MOPED algorithm (Heavens et al. 2000) to determine the star formation history of the galaxies. Third, we used the published ages by Bernardi et al. (2006a) that use stacked spectra of galaxies with similar properties to measure the absorption feature produced by the Balmer absorption lines (e.g.  $H\gamma_F$ ). Ages are then computed from the lines assuming  $\alpha$ -enhancement with respect to the solar abundance stellar population models. The first and third method return a luminosity-weighted age, while the MOPED technique, because it reconstructs the star formation history, returns the age of the different stellar components, which can be used to compute the mass-weighted age for the galaxy as a whole. The three methods are compared in detail in a companion paper by Jimenez et al. (2006).

There are about 22,000 galaxies in common between the MOPED sample (Panter et al. 2006) and the Bernardi et al. (2006a) sample. In Fig. 1, we show the age distribution for several velocity dispersions that we obtained for these galaxies. The solid (black) histograms show the mass-weighted age distributions from MOPED. The ages correspond to those extrapolated to  $z = 0$ ; note that we impose a prior that the age of any galaxy, when extrapolated to  $z = 0$ , cannot exceed 13.7 Gyr (Spergel et al. 2006). The distributions are broad for all values of  $\sigma_v$ , but are narrower for higher  $\sigma_v$ , and centered on older ages. The uncertainties due to age-measurement errors are shown by the error bars in the figure, and will be discussed in § 4 below.

For comparison, the blue (dashed) histograms show the age-distributions obtained from absorption line indices. As the fig-

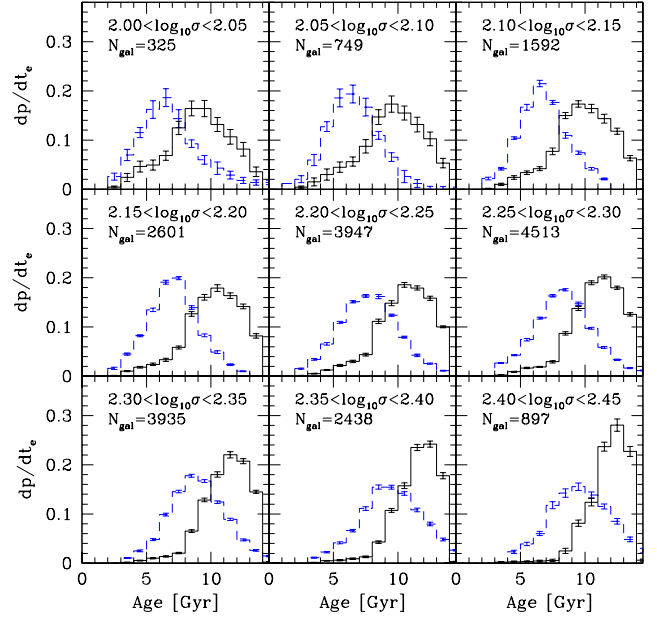


FIG. 1.— The distribution of stellar ages of early-type galaxies, as a function of their velocity dispersion  $\sigma_v$  in the range  $100 \text{ km s}^{-1} \lesssim \sigma_v \lesssim 280 \text{ km s}^{-1}$ . The spectra of  $\sim 22,000$  galaxies, all from  $z < 0.25$ , were used from SDSS DR4. Each  $\sigma_v$ -bin contains between  $\sim 300$  and  $\sim 4500$  galaxies, as labeled. The solid (black) histograms show the mass-weighted distributions inferred from the full spectra (continuum+lines) that we utilized in our analysis. Note that galaxies with larger  $\sigma_v$  are not only older, they have a narrower age-distribution. The dashed (blue) histograms show, for comparison, the age-distributions derived from absorption line indices. This method generally gives shorter ages (see text for discussion).

ure shows, the mean ages are lower, and the shapes of the distributions are different, from the MOPED results. These differences are partly accounted for by the mass vs. luminosity weighting, and by the fact that the MOPED ages do not include a correction for  $\alpha$ -enhancement. Full spectral models for the continuum+line emission, including  $\alpha$ -enhancement, are not available, but we expect that such models would somewhat reduce the inferred ages. There appear to be additional differences between the two age-measurement techniques (see Jimenez et al. 2006 for further discussion). We chose to adopt the MOPED age-distributions in our analysis below, because they utilize more information from the spectrum, and because they can be used to compute mass-weighted ages. We will discuss in § 5 below how our results would change if the ages inferred from the absorption-line indices were used instead.

## 3. RECONSTRUCTING THE QUASAR LUMINOSITY FUNCTION

We use the age-distribution of the early-type galaxies, inferred in § 2 above, to reconstruct the evolution of the quasar luminosity function, using the following simple assumptions.

We start with the velocity function of early-type galaxies at  $z \approx 0$ , as determined by Sheth et al. (2003),

$$\frac{dN}{d\sigma_v} d\sigma_v = 1.34 \times 10^{-3} (h_{70}^{-1} \text{ Mpc})^{-3} \left( \frac{\sigma_v}{88.8 \text{ km s}^{-1}} \right)^{6.5} \times \exp \left[ - \left( \frac{\sigma_v}{88.8 \text{ km s}^{-1}} \right)^{1.93} \right] \frac{d\sigma_v}{\sigma_v}. \quad (1)$$

This function, shown by the dashed curve in Figure 2, shows a clear peak: the abundance of early type galaxies declines at

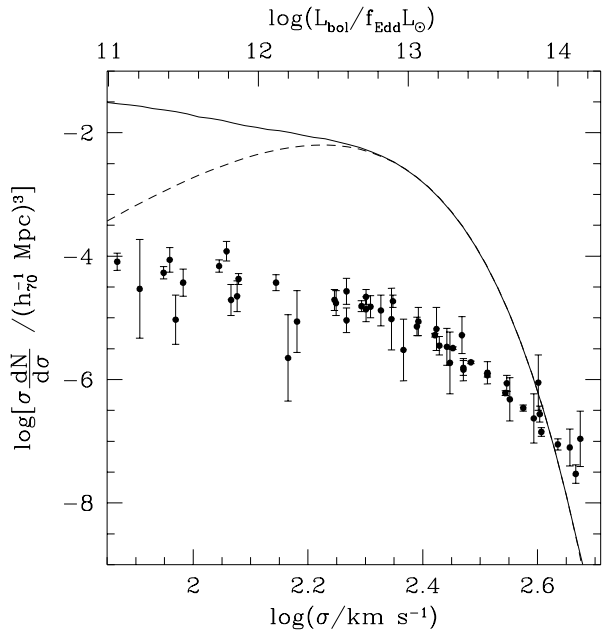


FIG. 2.— The local velocity function spheroids, adapted from Sheth et al. (2003), showing the contribution of early type galaxies (dashed curve), and the whole spheroid population, including the bulges of late type galaxies (solid curve). For comparison, the data-points show the quasar luminosity function at redshift  $z = 2.18$  (adapted from Hopkins et al. 2006). The upper horizontal axis labels show the mean quasar luminosity corresponding to  $\sigma_v$  from equation (3), which assumes that the BHs follow the  $M_{\text{bh}} - \sigma_v$  relation, and shine at a fraction  $f_{\text{Edd}}$  of the Eddington luminosity.

velocity dispersions below  $\lesssim 200 \text{ km s}^{-1}$ . Below this value, the population of spheroids is dominated by the bulges of late-type galaxies, as demonstrated by the solid curve showing the sum of the two spheroid velocity functions. For reference, the data-points in the figure show the observed quasar LF at redshift  $z = 2.18$  (adapted from Hopkins et al. 2006), using the mean  $L_Q - \sigma_v$  relation from equation (3) without any scatter. It is clear from the figure that the quasar LF at faint luminosities is monotonic, and traces the total spheroid population much more closely than the subset represented by the early type galaxies. The empirical evidence listed in the Introduction also suggests that the correlation between SMBH mass and spheroid properties apply both to SMBHs in early type galaxies and to those in bulges of late-type galaxies; it is therefore important to include late-type bulges in our analysis. Unfortunately, we do not have a direct measurement of the age-distribution of these bulges as a function of their velocity dispersion. However, bulges lie very close to the fundamental plane of elliptical galaxies, and appear to have similar formation epochs (Falc3n-Barroso et al. 2002); we therefore make the reasonable assumption that the age-distribution of a bulge is identical to that of an early-type galaxy with the same velocity dispersion. Furthermore, we follow Sheth et al. (2003) and identify  $\sigma_v = V_c/\sqrt{2}$  as the bulge velocity dispersion for a late-type galaxy with circular velocity  $V_c$ . This identification is justified by a recent, more detailed population synthesis study (Tundo et al. 2006).

We next assume that the stars in each of the nearby spheroid formed in a single burst, with the age  $t_e$  identified as the mass-weighted stellar age, inferred from the spectral fits of early-type galaxies discussed above. Both the mean age, and the shape of the age-distribution, are found to be a strong function

of the velocity dispersion  $dp/dt_e = dp/dt_e(\sigma_v, t_e)$  (see Figure 1 above).

We also assume that the velocity dispersion  $\sigma_v$  remains constant after the formation of the galaxy. Dry mergers between gas-poor early type galaxies may indeed cause only a modest change to  $\sigma_v$ , as expected based on idealized models and confirmed by numerical simulations (e.g. Nipoti et al 2003, although the precise conclusions depend on the merging galaxies' structure and their orbital parameters; Robertson et al. 2006, Boylan-Kolchin et al. 2006). If the BH masses add linearly, then such dry mergers cannot maintain the  $M_{\text{bh}} - \sigma_v$  relation, implying that mergers are either infrequent, or that they are accompanied by dissipation. Furthermore, in the high-resolution N-body simulations of Zhao et al. (2003a,b), dark matter halos grow in two phases. An initial rapid merger of many progenitors with comparable masses build up the potential well; this is followed by a slower accretion of lower-mass satellites adding mass primarily to the outskirts of the halo, without affecting the central structure. Our modeling implicitly requires only that most of the BH mass is assembled (possibly in multiple mergers) within a small fraction of the Hubble time.

Under the assumption that a SMBH forms concurrently with the stars in each early-type galaxy, we then adopt the SMBH mass given by the relation,

$$\log\left(\frac{M_{\text{bh}}}{M_{\odot}}\right) = \alpha + \beta \log\left(\frac{\sigma_v}{200 \text{ km s}^{-1}}\right) \quad (2)$$

with  $\alpha = 8.15$  and  $\beta = 3.83$ . This is the mean relation obtained by Tundo et al. (2006) while allowing an intrinsic scatter in  $M_{\text{bh}}$  at fixed  $\sigma_v$  (determined to be  $\sim 0.2$  dex). Although current SMBH samples suffer from selection bias, Bernardi et al. (2006b) suggest that the  $M_{\text{bh}} - \sigma_v$  relation is unlikely to have been strongly affected. Wyithe (2006) recently found that an additional quadratic term in the right-hand side of equation (2),  $\beta_2[\log(\sigma/200 \text{ km s}^{-1})]^2$ , is required. Although the statistical significance of a nonzero  $\beta_2 > 0$  is modest ( $\approx 1 - 1.5\sigma$  depending on the sample used), we have repeated our analysis below using the best-fit model in Wyithe (2006), with  $(\alpha, \beta, \beta_2) = (8.05, 4.2, 1.6)$ , and have verified that our predictions for the quasar LF change by much less than their uncertainties.

We assume that the SMBHs gain most of their mass in a luminous short-lived phase, at the end of their rapid assembly. During this phase, they radiate at some fraction  $f_{\text{Edd}}$  of the Eddington limit of their final mass, for a duration  $t_Q$  years. During this time, the SMBH is identified as a luminous quasar with a fixed luminosity  $L_Q$ . We expect the lifetime to be of order the Salpeter time,  $t_Q \sim 4 \times 10^7 \text{ yr}$  (Martini 2004; see also Shankar et al. 2004). Note that this lifetime is identified as the cumulative duration of quasar activity (i.e., if the activity is episodic, then it represents the sum of all episodes), and also assumes that the quasar is unobscured by gas or dust during the epoch of bright activity. This latter assumption may be justified in the scenario in which the lifetime is determined by feedback: the bright quasar epoch corresponds to an expulsion of the gas and dust from around the nucleus (which removes the obscuration on one hand, and terminates quasar activity on the other). This type of model of quasar activity has been proposed recently by Hopkins et al. (2005, and references therein), although we caution that in their model, the BHs spend a longer time in an obscured phase (see discussion in § 5 below).

While it is useful to think in terms of separate  $M_{\text{bh}} - \sigma_v$  and  $L_Q - M_{\text{bh}}$  relations (the latter specified by  $f_{\text{Edd}}$ ), both of which have been empirically constrained in various galaxy samples,

our model predictions depend only on the combination of these two, i.e. on the dependence of the quasar's luminosity  $L_Q$  on  $\sigma_v$ . We therefore introduce the parameter  $\alpha_L$  giving the normalization of the  $L_Q - \sigma_v$  relation for a SMBH in a host with velocity dispersion  $200 \text{ km s}^{-1}$ . We then have the bolometric luminosity

$$\log\left(\frac{L_Q}{L_\odot}\right) = \alpha_L + 12.72 + \beta \log\left(\frac{\sigma_v}{200 \text{ km s}^{-1}}\right), \quad (3)$$

where  $10^{4.57} L_\odot / M_\odot$  is the Eddington luminosity, so that  $\alpha_L = 0$  corresponds to the Eddington luminosity of a  $10^{8.15} M_\odot$  black hole, i.e. to the adopted normalization of the  $M_{\text{bh}} - \sigma_v$  relation and  $f_{\text{Edd}} = 1$ . In our analysis, we allow the normalization  $\alpha_L$  to vary with redshift; however, we keep the logarithmic slope fixed,  $d \log L_Q / d \log \sigma_v = \beta = 3.83$ .

Under the above assumptions, and in the limit of a negligible scatter in  $L_Q$  at fixed  $\sigma_v$ , the space density of luminous quasars at redshift  $z$  is predicted to be

$$\frac{dN^0}{dL_Q}(z) = \left(\frac{dN}{d\sigma_v}\right) \left[ t_Q \times \frac{dp}{dt_e}(\sigma_v, t_e) \right] \left(\frac{dL_Q}{d\sigma_v}\right)^{-1}. \quad (4)$$

In the above equation,  $t_e$  is the lookback time to redshift  $z$ ,  $dp/dt_e$  is unresolved and assumed to be a constant in each age bin of width  $dt_e = 1 \text{ Gyr}$ , and  $L_Q$  is the bolometric luminosity given by equation (3).

Since the  $M_{\text{bh}} - \sigma_v$  relation and  $f_{\text{Edd}}$  are both likely to have intrinsic scatter, we allow a probability distribution  $dp/dL_Q$  of quasar luminosities at fixed  $\sigma_v$ . To be specific, we assume that  $dp/dL_Q$  follows a log-normal distribution, i.e.  $dp/d \log L_Q$  is described by a Gaussian,<sup>1</sup> with a width independent of  $L_Q$ . This can be achieved by allowing  $\alpha_L$  to have a Gaussian distribution with a mean  $\langle \alpha_L \rangle$  and standard deviation  $\Delta \alpha_L$ .<sup>2</sup>  $\Delta \alpha_L$  can therefore be regarded as the combined scatter in the  $M_{\text{bh}} - \sigma_v$  relation (at fixed  $\sigma_v$ ) and in  $f_{\text{Edd}}$  (at fixed  $M_{\text{bh}}$ ). To predict the quasar LF in the presence of scatter, the quantity in equation (4) has to be convolved with  $dp/dL_Q$ ,

$$\begin{aligned} \frac{dN}{d \log L_Q} &= \int_0^\infty d \log L_Q^0 \frac{dN^0}{d \log L_Q^0} \frac{dp}{d \log L_Q} \Big|_{\log L_Q^0} \\ &= \int_0^\infty d \log L_Q^0 \frac{dN^0}{d \log L_Q^0} \frac{dp}{d \alpha_L}. \end{aligned} \quad (5)$$

In these equations,  $\log L_Q^0$  represents a mean logarithmic luminosity, computed from equation (3) with  $\alpha_L = \langle \alpha_L \rangle$ , and in the last equation, the Gaussian  $dp/d \alpha_L$  is evaluated at  $\alpha_L = \log L_Q - \log L_Q^0$ .

In summary, the parameters of the model described above are  $t_Q$ ,  $\langle \alpha_L \rangle$ , and  $\Delta \alpha_L$ , describing the duration of quasar activity, and the mean luminosity and its scatter during the quasar epoch of a SMBH in a spheroid with fixed  $\sigma_v$ . We will fit these three parameters simultaneously and independently in each redshift bin, i.e. we do not require a priori that these parameters be redshift-independent. We note again that for comparison to previous work, it can be useful to regard the  $L_Q - \sigma_v$  relation we use in our fits as the combination of an  $M_{\text{bh}} - \sigma_v$  relation and the Eddington ratio  $f_{\text{Edd}}$ .

#### 4. COMPARING PREDICTED AND OBSERVED QUASAR LFS

Our main task is to compare the predictions of the above model to the observed quasar LF. The bolometric quasar LF has

<sup>1</sup> Note that here and elsewhere in the paper,  $\log$  refers to base 10 logarithm.

<sup>2</sup> Note that with this definition  $\langle L_Q \rangle \neq 10^{\langle \alpha_L \rangle}$ . Our definition is consistent with Tundo et al. (2006), i.e. equation (2) describes the logarithmic mean  $\langle \log M_{\text{bh}} \rangle$ .

been recently inferred from a compilation of multi-wavelength data (Hopkins et al. 2006). Here we adopt the observational data-points, with their quoted statistical errors, as reported in this compilation, but re-binned to correspond to the LF in 12 different redshift intervals, centered at look-back times of  $t = 1.5 - 12.5 \text{ Gyr}$ , in increments of 1 Gyr. Each redshift bin has a width corresponding to  $\Delta t = \pm 0.5 \text{ Gyr}$ . These data, together with their errors, are shown in both Figures 3 and 4.

In order to compare our model predictions to these data, several additional uncertainties need to be taken into account. In determining the fraction of galaxies, at fixed  $\sigma_v$ , that fall within a given age bin, there are two main sources of errors. First, there is a Poisson sampling error  $\delta n_p$ , which is significant in those age- and  $\sigma$ -bins that have only a few galaxies (the number of galaxies is indicated by the label in each panel in Fig. 1). Second, errors in the age determinations (increasing from  $\delta t_e < 1 \text{ Gyr}$  for  $t_e \lesssim 7 \text{ Gyr}$  to  $\delta t_e \approx 3 \text{ Gyr}$  for  $t_e \gtrsim 10 \text{ Gyr}$ ) can shift galaxies between age-bins. We estimated this error,  $\delta n_t$ , by performing 20 Monte Carlo realizations of each of the age-distributions, generating a random age of each galaxy within its allowed range returned by MOPED. We maintain the prior that the age of any galaxy, when extrapolated to  $z = 0$ , cannot exceed 13.7 Gyr, and identify  $\delta n_t$  as the range that includes 14 out of the 20 realizations. The resulting uncertainties  $\delta n_t$  are shown by the error-bars in Figure 1. We add  $\delta n_p$  and  $\delta n_t$  in quadrature, to obtain the total uncertainty in the fraction of galaxies falling in each age-bin.

In obtaining the total (normalized) space density of quasars, there is an additional uncertainty, from the measurement errors of the local velocity function of early type galaxies (Sheth et al. 2003). The statistical errors are small ( $\lesssim 15\%$ , although they increase toward the bright end), and systematic errors, due to including/excluding low S/N galaxies, are somewhat larger, 20-25%. We chose to include an additional, independent 15% error in each luminosity bin in the quasar space density, although we note that in practice, these errors are much smaller than the combination of the other two sources of error and the observational errors, discussed in the preceding paragraphs.

Finally, there is additional uncertainty in the prediction of the quasar LF at the faint end (corresponding to the threshold  $\sigma_v \approx 100 \text{ km/s}$ ) in those models with a large scatter ( $\Delta \alpha_L \gtrsim 0.5$ ). In these models, the velocity function, and the age distributions, have to be extrapolated to  $\sigma_v < 100 \text{ km/s}$ . While the uncertainty introduced by this extrapolation cannot be rigorously quantified, we include it in our error budget as follows. We first compute the quasar LF in the absence of scatter,  $N_Q^0 \equiv L_Q(dN^0/dL_Q)$ , by extrapolating the power-law slope implied by equation (4), and convolve  $N_Q^0$  with the given scatter  $\Delta \alpha_L$  following equation (5). We then repeat this calculation, but reducing/increasing  $dp/dt_e$  in each  $t_e$  bin by its  $1\sigma$  uncertainty as discussed above. This results in a flatter/steeper slope for  $N_Q^0$ , and yields a lower/higher  $N_Q$ . We adopt these values as the  $1\sigma$  lower/upper limits on  $N_Q$ . In practice, this increases the Poisson error on  $\Delta N_Q$  significantly in models with scatter relative to those with no scatter. As an example, at  $z = 0.31$ , at the faintest  $L$  the uncertainty is a factor of  $\sim 3$  without scatter (shown in Fig. 3), but is about a factor of  $\sim 6$  for the model with  $\Delta \alpha_L = 0.6$  (shown in Fig. 4).

In summary, given a set of parameters,  $t_Q$ ,  $\langle \alpha_L \rangle$ , and  $\Delta \alpha_L$ , we compute the expected space density of quasars in each logarithmic luminosity bin,  $N_Q$  as described in the previous section, and at each redshift and luminosity, we compute the error  $\Delta N_Q$

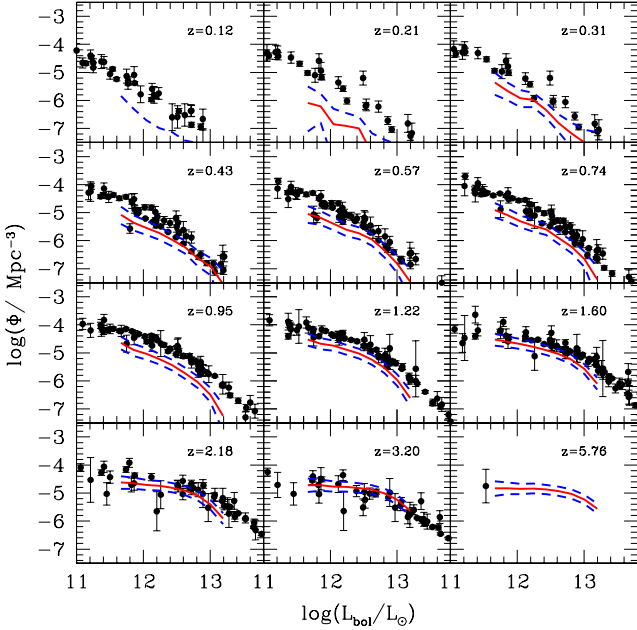


FIG. 3.— This figure shows the predicted and observed quasar LF at 12 different redshifts, as labeled (corresponding to look-back times of 1.5–12.5 Gyr, in increments of 1 Gyr). The solid (red) curves follow from a model with  $L_Q - \sigma_v$  normalization  $\alpha_L = 0$  (which corresponds to  $f_{\text{Edd}} \equiv L_Q/L_{\text{Edd}} = 1$  with our adopted  $M_{\text{bh}} - \sigma_v$  normalization). The model assumes no scatter, and a quasar phase that lasts for a Salpeter time at a radiative efficiency of 10 percent ( $t_Q = 4 \times 10^7$  years). The dashed (blue) curves indicate the uncertainty in the model prediction, arising from Poisson sampling, age-determination, and local galaxy abundance errors (in the top left panel, only the upper limit is visible). The black data-points have been adapted from a recent compilation by Hopkins et al. (2006).

by adding in quadrature the Poisson sampling errors, the errors caused by the age-determinations, and the uncertainties in the local galaxy abundance. We then compute a  $\chi^2$  for each data-point in the Hopkins et al. (2006) compilation that falls within the predicted range of luminosities. Here  $\chi^2$  is defined as the ratio  $\Delta N_{Q,\text{diff}} / \Delta N_{Q,\text{err}}$ , where  $dN_{Q,\text{diff}}$  is the difference between the predicted and measured quasar space densities, and  $dN_{Q,\text{diff}}$  is the sum in quadrature of the modeling errors and the observational errors discussed above. Note that the number of data-points available for the comparison of predictions vs. observations (and hence the number of degrees of freedom in the fit) varies with  $\langle \alpha_L \rangle$ . This is because  $\sigma_v$  lies in the range  $100 \text{ km s}^{-1} \lesssim \sigma_v \lesssim 280 \text{ km s}^{-1}$ , but the corresponding range of  $L_Q$  shifts with  $\alpha_L$ .

At each redshift, the above procedure yields a total  $\chi^2$ , summed over the available observational data-points, as a function of  $t_Q$ ,  $\langle \alpha_L \rangle$ , and  $\Delta \alpha_L$ . As a single figure of merit for the goodness-of-fit of a model, we further sum the total  $\chi^2$  over all of the 12 redshift bins, and obtain a cumulative reduced  $\chi^2$  (where the number of degrees of freedom, i.e. the number of data-points, minus 3 for the 3 independent fitting parameters, is typically of order  $\sim 100$ ).

## 5. RESULTS AND DISCUSSION

In Figures 3 and 4, we show the predicted quasar LF at 12 different redshifts, compared to the observed bolometric LF adapted from the compilation by Hopkins et al. (2006; shown as black points with error-bars). The twelve different panels correspond to 1 Gyr-wide bins in look-back times, centered on

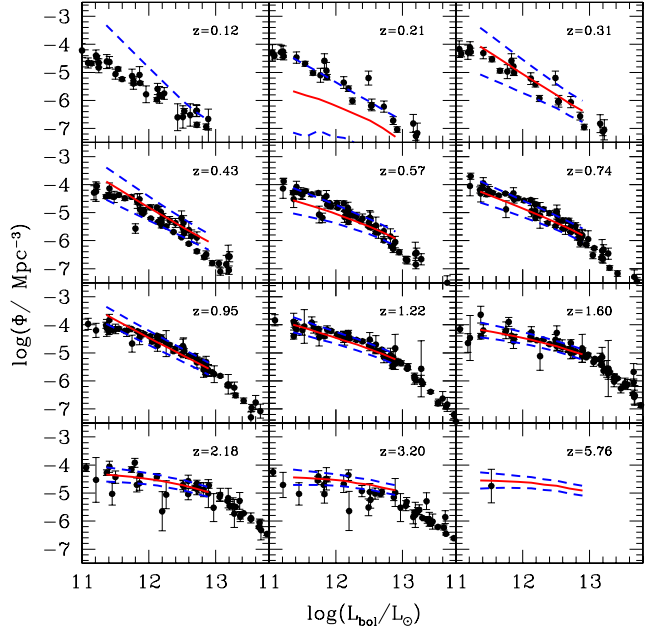


FIG. 4.— This figure shows the predicted and observed quasar LF at 12 different redshifts, together with their uncertainties, as in Figure 3. The curves here assume  $\alpha_L = -0.3$  (corresponding to a constant, redshift-independent mean Eddington ratio of  $\langle \log f_{\text{Edd}} \rangle = -0.3$  with our adopted  $M_{\text{bh}} - \sigma_v$  normalization), a scatter of 0.6 dex in  $L_Q$  at fixed  $\sigma_v$ , and a quasar lifetime of  $8 \times 10^7$  years. This model a statistical fit with a reduced  $\chi^2$  of 1.1 (see text for discussion), for the entire redshift range as a whole. Note that the presence of scatter increases the uncertainties relative to Figure 3.

$t_e = 1.5 - 12.5$  Gyr, in increments of 1 Gyr, and to redshifts as labeled. The curves in Figure 3 have been obtained in a “basic” model with the most naïve set of assumptions, namely  $\alpha_L = 0$  with no scatter, and a quasar phase lasting for a Salpeter time at a radiative efficiency of 10 percent ( $t_Q = 4 \times 10^7$  years). This model is shown for illustration. The solid (red) curves show the predicted quasar LF, and the dashed (blue) curves bracket the estimated  $1\sigma$  uncertainties, as discussed in § 4 above.

As the figure shows, this naïve model under-predicts the overall normalization of the LF (especially at low redshifts), and predicts a shape that declines too steeply at the bright end (especially at high redshift). Therefore, under the most naïve assumptions, the age-distributions we infer for the early-type populations do not “map” the local population of early-type galaxies onto the evolving quasar population. The age-distributions have the right property, in that larger early-types are older (as inferred by numerous previous works on “down-sizing”). This is in accord with the increase in the characteristic quasar luminosity toward high  $z$  (e.g. Cattaneo & Bernardi 2003; Haiman, Ciotti & Ostriker 2004). However, over the range of velocity dispersions  $100 \text{ km s}^{-1} < \sigma_v < 280 \text{ km s}^{-1}$  for which we can determine the age-distribution, the corresponding quasar LF flattens considerably from  $z = 0$  to  $z = 2 - 3$ . This flattening is not reproduced by the dependence of the observed age-distribution on  $\sigma_v$ .

We have searched through the full 3-dimensional parameter space ( $t_Q$ ,  $\langle \alpha_L \rangle$ ,  $\Delta \alpha_L$ ) for a set of values that corrects these deficiencies. Changes in  $t_Q$  and  $\langle \alpha_L \rangle$  amount to shifting the predicted LF along the vertical or horizontal axes in Figure 4, respectively, without changing the predicted shape. An increased scatter (higher  $\Delta \alpha_L$ ) also shifts the LF up along the vertical

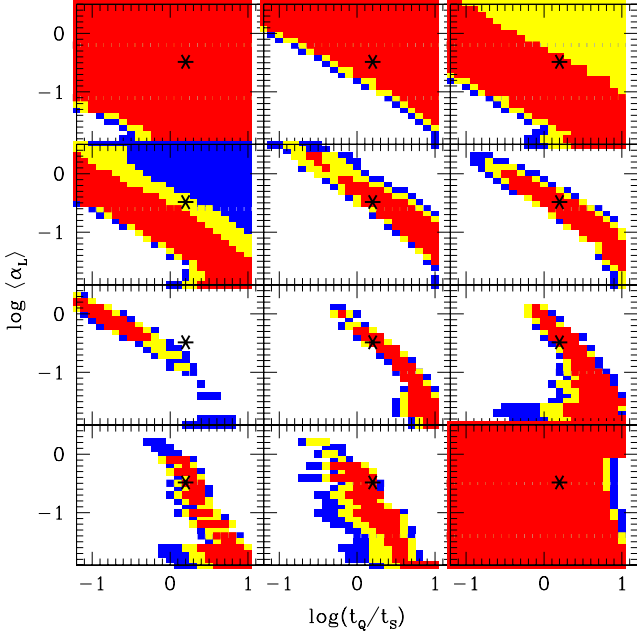


FIG. 5.— This figure shows, in each redshift bin, contours of constant reduced  $\chi^2$  in that bin. The blue/yellow/red contours correspond to  $\chi^2 = 2.0, 1.5$ , and  $1.0$ . The x-axis in each panel shows the quasar lifetime in units of the Salpeter time,  $4 \times 10^7$  yr, and the y-axis shows the mean  $\alpha_L$  (equivalent to the mean Eddington ratio with our adopted  $M_{\text{bh}} - \sigma_v$  normalization). The scatter in all models are fixed at  $\Delta\alpha_L = 0.9$ .

axis, but it also flattens the predicted LF, by preferentially increasing the abundance at the bright, steep tail.

The solid (red) curves in Figure 4 show predictions from a model with parameter choices of  $(t_Q, \langle\alpha_L\rangle, \Delta\alpha_L) = (8 \times 10^7 \text{ years}, -0.3, 0.5)$ . This model has a reduced  $\chi^2$  of  $1.1$  ( $\chi^2 = 106$  for 98 degrees of freedom over the twelve redshift bins). The dashed curves indicate the uncertainty in the model predictions in each age bin. The uncertainty increases at the faint end of the LF, and at lower redshifts (as well as in the highest  $z$  bin), as there are only a handful of SDSS galaxies in these velocity dispersion and age bins (see Figure 1). As noted above, the predicted LF at the faint end has an additional uncertainty when the scatter is large, since the prediction involves extrapolating to  $\sigma_v < 100$  km/s.

This model, while simple, is in reasonable overall agreement with the observational data. There does not appear to be compelling evidence that either the duty cycle or the Eddington ratio (or  $M_{\text{bh}} - \sigma_v$  relation) evolves significantly with redshift. It is also worth pointing out that the quasar lifetime preferred by this model is about a factor of two longer than the fiducial Salpeter time of  $4 \times 10^7$  years (at a radiative efficiency of  $\epsilon = 0.10$ ).

In Figure 5, we assume a larger scatter of  $\Delta\alpha_L = 0.9$ , and we show contours of constant reduced  $\chi^2$  as a function of the other two parameters. The reduced  $\chi^2$  was computed separately in each of the redshift bins (each bin having  $\sim 10$  d.o.f. on average). The blue/yellow/red contours correspond to  $\chi^2 = 2.0, 1.5$ , and  $1.0$ , respectively, and the star in each panel marks the model that best fits when all 12 redshift bins are combined,  $(t_Q, \langle\alpha_L\rangle, \Delta\alpha_L) = (6.3 \times 10^7 \text{ years}, -0.5, 0.9)$ . As this figure shows, no combination of parameters can match the observed LF at the precision of  $\chi^2 < 1.5$  simultaneously at all redshifts (the worst fit is at  $z = 0.95$ , as we discussed above). On the other hand, the

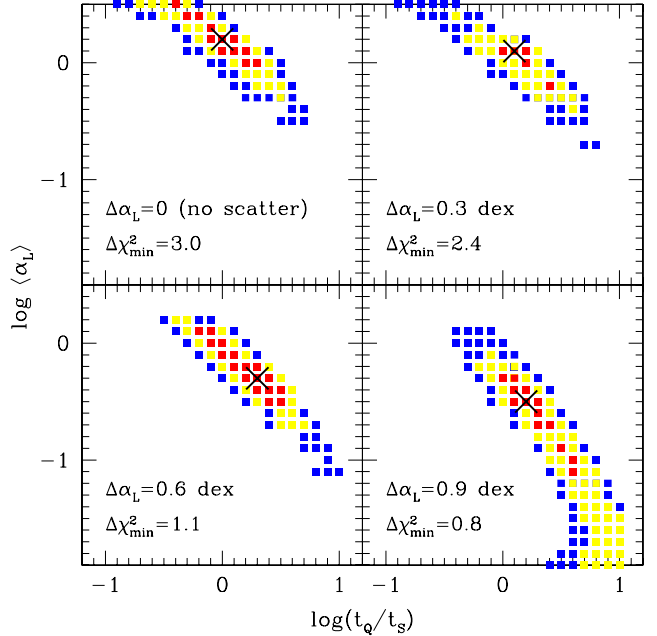


FIG. 6.— This figure shows contours of constant reduced  $\chi^2$  combined over all 12 redshift bins. The scatter is fixed at four different values ( $\Delta\alpha_L = 0, 0.3, 0.6, 0.9$ ). In each panel, the large cross marks the best-fit model. Note that the best-fit models have smaller reduced  $\chi^2$  when the scatter is increased. The contour levels in each panel are adjusted to the minimum of  $\chi^2$ , and are different in each panel. The blue/yellow/red contours enclose points with  $\chi^2$  below  $(4.0, 5.5, 8.0)$ ,  $(3.0, 5.0, 7.0)$ ,  $(2.0, 3.0, 4.0)$ , and  $(1.0, 1.5, 2.0)$  in the four panels, respectively (from top left, clockwise). These contours serve to illustrate the direction of the degeneracies discussed in the text, and show that a non-negligible scatter ( $\Delta \gtrsim 0.6$ ) is required.

figure shows significant degeneracies: roughly, a longer lifetime can be “traded” for a smaller  $\alpha_L$  (or equivalently, a smaller Eddington ratio). This is expected: a smaller  $\alpha_L$  shifts our predicted LF curves to the left (a given  $L_Q$  then corresponds to a larger  $\sigma_v$ , i.e. a smaller  $dn/d\sigma_v \times dp/dt_e$ ), while a longer lifetime moves the curves upward (scaling linearly). This explains the sense of the degeneracy for a given  $L_Q$ . Likewise, we found (not shown on the figure) that an increased scatter can be compensated by a shorter lifetime and/or a smaller Eddington ratio.

Overall, there is a suite of models that can fit the LF over most of the redshift range. In particular, models along lines with  $\log t_Q + \langle\alpha_L\rangle \approx \text{constant}$  are degenerate, with models with longer lifetimes only mildly disfavored. For example, the models with  $(t_Q, \langle\alpha_L\rangle, \Delta\alpha_L) = (6.3 \times 10^7 \text{ years}, -0.5, 0.9)$  or  $(1.6 \times 10^8 \text{ yr}, -1.6, 1.2)$  both have overall reduced  $\chi^2 \lesssim 1.0$  (with all twelve redshift bins combined). We find that models with even larger scatter can have even smaller reduced  $\chi^2$ ; this is a result of the large prediction uncertainty in these models. Such large-scatter models, with somewhat longer lifetimes, however, require exceedingly small  $\alpha_L$ , or equivalently, small Eddington ratios ( $\lesssim 0.03$ ), and are disfavored by other considerations (see discussion below).

In Figure 6, we show contours of constant reduced  $\chi^2$  with all 12 redshift bins combined. The four panels fix the scatter at four different values ( $\Delta\alpha_L = 0, 0.3, 0.6, 0.9$ ). In each panel, the large cross marks the best-fit model. As explained above, the models with large scatters have best-fits with lower reduced  $\chi^2$ , shown in each panel. As the figure shows,  $\Delta\alpha_L < 0.6$  yields poor fits. We therefore find that the fits require a non-negligible scatter;

this is a result of the quasar LF being flatter at the bright end then the velocity–function of spheroids (as seen clearly in Figure 2). The contour levels in each panel are adjusted to the minimum of  $\chi^2$ , and are different in each panel. The blue/yellow/red contours enclose points with  $\chi^2$  below (4.0, 5.5, 8.0), (3.0, 5.0, 7.0), (2.0 3.0 4.0), and (1.0 1.5 2.0) in the four panels, respectively (from top left, clockwise). These contours serve to illustrate the direction of the degeneracies discussed above.

We note that our conclusions above are based on the mass-weighted stellar age as a proxy for the time the SMBH forms. The mass-weighted age is likely to be the appropriate estimate, if the bulk of the stars and the SMBH forms concurrently. However, to check the sensitivity of our results to this assumption, we have repeated our analysis, replacing the mass-weighted age either by a luminosity-weighted age, or an alternative age-estimate based on the ( $H\gamma_F$ ) absorption line index. In both cases, we find that the ages are decreased (the decrease is more pronounced when the absorption-line ages are used). This increases the predictions for the quasar LF at low redshifts ( $z \lesssim 1$ ), and, as a result, we find that matching the observed LF would require that either  $\langle\alpha_L\rangle$ ,  $\Delta\alpha_L$ , and/or  $t_Q$  decline from  $z \approx 2$  to  $z = 0$  by a factor of a few. One or more of the three model parameters would therefore have to evolve to fit the quasar LF over the entire range  $0 < z \lesssim 6$ .

Our result also assumes that the luminous quasar phase is short, and it follows promptly the formation of the SMBH. The accretion history and the corresponding “lightcurve” of SMBHs can be more extended and complex. We first note that in the best-fit models we find with reduced  $\chi^2 \sim 1$ , the quasar lifetime is a factor of 1.5–2 longer than the Salpeter time, while the mean Eddington ratio is 0.3–0.5. At fixed radiative efficiency, this implies that during the quasar phase, the BH mass, and the accompanying luminosity, increases by a factor of  $\sim 2$ . In our models, we ignored this increase, and assumed a constant  $L_Q$  during the luminous phase. In practice, such a variation in  $L_Q$  would mimic a smaller Eddington ratio and a larger scatter in our models. Given the uncertainties about the actual quasar light-curve, we chose not to model this variation here.

Observations of X-ray spectra (e.g. Wall et al. 2005; Barger et al. 2005) suggest that a SMBHs can suffer significant obscuration, an effect that increases at lower luminosities. For example, Cattaneo & Bernardi (2003) included a luminosity-dependent obscuration in their predictions for the quasar LF. In their model, the evolution of bright quasars is determined by the age-distribution, but the evolution of faint quasars is driven by the assumed form of the obscuration (which reduces the abundance of faint quasars). They showed that the obscuration can achieve the required flattening of the LF (which, in our case, is attributed to scatter instead). On the other hand, the X-ray observations, and also theoretical arguments (Hopkins et al. 2005, 2006) suggest that SMBHs spend a significantly longer period in their obscured phase, during which they shine well below the Eddington luminosity. Such a luminosity-dependent lifetime would further change the shape of the predicted LF, and would likely require the introduction of a more detailed model, in which  $t_Q$ ,  $\langle\alpha_L\rangle$  and  $\Delta\alpha_L$  depend on the SMBH mass.

Taken at face value, however, our results imply that the duty cycle, the Eddington ratio, and the  $M_{\text{bh}} - \sigma_v$  relation, do not necessarily evolve with redshift. Our results do not, conversely, imply that evolution is ruled out. For example, one could adopt different points from the degenerate innermost red contours shown in Figure 3 at each redshift. Alternatively, Figure 6 shows that

the best-fit values of  $\langle\alpha_L\rangle$  and  $t_Q$  do change as scatter is varied; one could therefore postulate an evolving  $\langle\alpha_L\rangle$  (say, decreasing with redshift) together with an evolving scatter (which would have to then increase with redshift).

There have been suggestions in the recent literature that the normalization of the  $M_{\text{bh}} - \sigma_v$  relation may increase toward high  $z$ , with  $M_{\text{bh}}$  larger at fixed  $\sigma_v$  (e.g. Shields et al. 2006; Wandel 2004) – by as much as a factor of 4 at  $z = 0.36$  than at  $z = 0$  (Woo et al. 2006), although these results could arise from a selection effect of preferentially missing the lower luminosity BHs at high  $z$ , or the high luminosity BHs at low  $z$  (Bernardi et al. 2006b).

Eddington ratios are difficult to determine empirically (although this could be possible in the future with high precision, if gravity waves can be detected by LISA and identified with luminous quasars; Kocsis et al. 2006). Kollmeier et al. (2006) combined measurements of line widths and continua of a sample of AGN at  $0.3 < z < 4$  to infer  $\langle f_{\text{Edd}} \rangle \sim 0.3$ , with a scatter of  $\sim 0.3$  dex, with no apparent evolution in the mean or the scatter (note that if the fueling rate falls below the Eddington rate, it would be surprising if it had no scatter). Vestergaard (2004) estimated Eddington ratios in a sample of high redshift quasars using an observed correlation between the size of the broad line region and the luminosity of the quasar (the correlation is calibrated using reverberation mapping of lower redshift objects; e.g. Kaspi et al. 2000; Vestergaard 2002). They find values ranging from  $\approx 0.1$  to  $\gtrsim 1$ , with the  $z \gtrsim 3.5$  quasars having a somewhat higher mean  $L/L_{\text{Edd}}$ , and a narrower distribution, than the lower redshift population. In a more extensive lower redshift  $0 < z < 1$  sample, Woo & Urry (2002) also find higher Eddington ratios towards  $z = 1$ . However, these results may represent a trend towards higher ratios at higher luminosities, and could also be explained by selection effects. Whether there exists any trend, and whether it is primarily with redshift or luminosity is an important question, but large scatter and selection effects presently preclude a firm answer.

Our fits are in good agreement with these Eddington ratio measurements. Our results suggests that, in order to flatten the predicted quasar LF at  $z = 2 - 3$ , a scatter *must* be present in the relation between  $L$  and  $\sigma_v$ . Tundo et al. (2006) find an intrinsic scatter of  $\approx 0.22$  dex, while Wyithe (2006) and Marconi and Hunt (2004) both find 0.3 dex, in the  $M_{\text{bh}} - \sigma_v$  relation, and Lapi et al. (2006) find a similar scatter of 0.3 dex in  $M_{\text{BH}}$  at fixed virial mass. The combined scatter in the  $M_{\text{bh}} - \sigma_v$  relation (0.2–0.3 dex) and in  $f_{\text{Edd}}$  (0.3 dex from Kollmeier et al.), when added in quadrature, is  $\sim 0.4$  dex, which is in fair agreement with our finding that  $\gtrsim 0.6$  dex is required (for a reduced  $\chi^2$  of 1.1 or smaller, see Figure 6). However, it is interesting to note that our minimum scatter is slightly larger than the combined scatter in the  $M_{\text{bh}} - \sigma_v$  relation and  $f_{\text{Edd}}$ , and a factor of 3 larger than the scatter in the  $L_* - \sigma_v$  relation of early-type galaxies, which is  $\sim 0.2$  dex.

## 6. CONCLUSIONS

In this paper, we attempted to predict the evolution of the optical quasar luminosity function, over the redshift range  $0 < z \lesssim 6$ , in a simple model with three free parameters, which is based on the inferred age-distribution of early type galaxies, and makes the assumption that quasar black hole growth and star-formation track one another at all times. Our “best-fit” models have quasar lifetimes ( $\approx 6 - 8 \times 10^7$  yr), mean Eddington ratios ( $\approx 0.3 - 0.5$ ) that are in good agreement with other

determinations. Our results also require a non-negligible scatter between the velocity dispersion of the galaxy and the mass of its resident BH ( $\approx 0.6-0.9$  dex). Our basic conclusion is that the quasar LF can be fit to satisfactory accuracy in these simple models, without a compelling need for any of the model parameters to evolve with redshift between  $0 < z \lesssim 6$ . This result supports the direct connection between the build-up of spheroids and their nuclear SMBHs.

We are grateful to Philip Hopkins for providing the re-binned data-points for the quasar LF in Figure 4, and an anonymous referee whose comments helped to significantly improve this paper. ZH acknowledges partial support by NASA through grants NNG04G188G and NNG05GF14G, by the NSF through grants AST-0307291 and AST-0307200, and by the Hungarian Ministry of Education through a György Békésy Fellowship. RJ is partially supported by NSF grant PIRE-0507768 and NASA grant NNG05GG01G. MB is partially supported by NASA grant LTSA-NNG06GC19G, and by grants 10199 and 10488 from the Space Telescope Science Institute, which is operated by AURA, Inc., under NASA contract NAS 5-26555.

#### REFERENCES

- Barger, A. J., Cowie, L. L., Mushotzky, R. F., et al. 2005, *AJ*, 129, 578  
 Bernardi, M. 2006, *AJ*, submitted, astro-ph/0609301  
 Bernardi, M., Nichol, R. C., Sheth, R. K., et al. 2006a, *AJ*, 131, 1288  
 Bernardi, M., Sheth, R. K., Tundo, E. & Hyde, J. B. 2006b, *ApJ*, submitted (astro-ph/0609300)  
 Blanton, M., Cen, R., Ostriker, J. P., et al. 2000, *ApJ*, 531, 1  
 Boylan-Kolchin, M., Ma, C.-P., & Quataert, E. 2006, *MNRAS*, 369, 1081  
 Boyle, B. J., Shanks, T., Croom, S. M., Smith, R. J., Miller, L., Loaring, N., & Heymans, C. 2000, *MNRAS*, 317, 1014  
 Cattaneo, A., & Bernardi, M. 2003, *MNRAS*, 344, 45  
 Cavaliere, A., & Vittorini, V. 2002, *ApJ*, 570, 114  
 Ciotti, L., & van Albada, T. S. 2001, *ApJ*, 552, L13  
 Falcón-Barroso, J., Peletier, R. F., & Balcells, M. 2002, *MNRAS*, 335, 741  
 Ferrarese, L., Merritt, D. 2000, *ApJ*, 539, L9  
 Franceschini, A., Hasinger, G., Miyaji, T., Malquori, D. 1999, *MNRAS*, 310, 5  
 Gebhardt, K., et al. 2000, *ApJ*, 539, L13  
 Graham, A. W., Erwin, P., Caon, N., & Trujillo, I. 2001, *ApJ*, 563, L13  
 Granato, G. L., Silva, L., Monaco, P., Panuzzo, P., Salucci, P., De Zotti, G., & Danese, L. 2001, *MNRAS*, 324, 757  
 Granato, G. L., De Zotti, G., Silva, L., Bressan, A., & Danese, L. 2004, *ApJ*, 600, 580  
 Haiman, Z., Ciotti, L., & Ostriker, J. P. 2004, 606, 763  
 Haiman, Z., & Loeb, A. 1998, *ApJ*, 503, 505  
 Haiman, Z., & Menou, K. 2000, *ApJ*, 531, 42  
 Heavens A. F., Jimenez R., & Lahav, O. 2000, *MNRAS*, 317, 965  
 Heavens A. F., Panter B., Jimenez R., Dunlop J. 2004, *Nature*, 428, 625  
 Hopkins, P. F., Hernquist, L., Cox, T. J., et al. 2005, *ApJ*, 632, 81  
 Hopkins, P. F., Hernquist, L., Cox, T. J., et al. 2006, *ApJS*, 163, 1  
 Kaspi, S., Smith, P. S., Netzer, H., Maoz, D., Jannuzi, B. T., & Giveon, U. 2000, *ApJ*, 533, 631  
 Kauffmann, G. & Haehnelt, M. 2000, *MNRAS*, 311, 576  
 Kocsis, B., Frei, Zs., Haiman, Z., & Menou, K. 2006, *ApJ*, 637, 27  
 Kollmeier, J. A. et al. 2006, *ApJ*, submitted, astro-ph/0508657  
 Lapi, A., et al. 2006, *ApJ*, submitted, astro-ph/0603819  
 Magorrian, J., et al. 1998, *AJ*, 115, 2285  
 Marconi, A., & Hunt, L. K. 2003, *ApJ*, 589, 21  
 Martini, P. 2004 in “Coevolution of Black Holes and Galaxies”, Carnegie Observatories Astrophysics Series, Vol. 1, Ed. L. C. Ho. (Cambridge, U.K.: Cambridge University Press), p. 169  
 Monaco, P., Salucci, P., & Danese, L. 2000, *MNRAS*, 311, 279  
 Nipoti, C., Londrillo, P., & Ciotti, L. 2003, 2003, *MNRAS*, 342, 501  
 Robertson, B., Cox, T. J., Hernquist, L., Franx, M., Hopkins, P. F., Martini, P., & Springel, V. 2006, *ApJ*, 641, 21  
 Shankar, F., Salucci, P., Granato, G. L., De Zotti, G. & Danese, L. 2004, *MNRAS*, 354, 1020  
 Sheth, R. K., Bernardi, M., Schechter, P., et al. 2003, *ApJ*, 594, 225  
 Shields, G. A., Menezes, K. L., Massart, C. A., & Vanden Bout, P. 2006, *ApJ*, 641, 683  
 Spergel, D. N. et al. 2006, *ApJ*, submitted, astro-ph/0603449  
 Tundo, E., Bernardi, M., Hyde J. B., Sheth, R. K., & Pizzella, A. 2006, *ApJ*, submitted, astro-ph/0609297  
 Vestergaard, M. 2004, *ApJ*, 601, 676  
 Wall, J. V., Jackson, C. A., & Shaver, P. A., et al. 2005 *A&A*, 434, 133  
 Wandel, A. 2004 in “Coevolution of Black Holes and Galaxies”, Carnegie Observatories Astrophysics Series, Vol. 1, Ed. L. C. Ho. (Cambridge, U.K.: Cambridge University Press), p. 65  
 Woo, J.-H., & Urry, C. M. 2002, 579, 530  
 Woo, J.-H., Treu, T., Malkan, M. A., & Blandford, R. D. 2006, *ApJ*, in press, astro-ph/0603648  
 Wyithe, J. S. B., 2006, *MNRAS*, 365, 1082  
 Wyithe, J. S. B., & Loeb, A. 2003, *ApJ*, 595, 614  
 York, D. G. 2000, *AJ*, 120, 1579  
 Zhao, D. H., Mo, H. J., Jing, Y. P., & Börner, G. 2003a, *MNRAS*, 339, 12  
 Zhao, D. H., Mo, H. J., Jing, Y. P., & Börner, G. 2003b, *ApJL*, 597, 9